Supplementary Material

Proton Migration Pathways and Hydrogen Evolution Mechanism in g-C_3N_4/TiO_2-B and Li-F Co-Doped Heterostructures From Theoretical Study

Shuhan Tang[a,‡], Qi Jiang[a,‡], Shuang Qiu[a], Hanyang Ji[a,b] and Xiaojie Liu[a,b,]*

[a]Center for Quantum Sciences and School of Physics, Northeast Normal University, Changchun, 130117, China.
[b]Center for Advanced Optoelectronic Functional Materials Research, and Key Laboratory of UV Light-Emitting Materials and Technology of Ministry of Educations, Northeast Normal University, Changchun, 130024, China
*Email: liuxj100@nenu.edu.cn
‡These authors contributed equally to this work.

Outline

1. Geometry models

Fig. S1 provides a comprehensive schematic overview of all relevant structural models. In principle, the g-C_3N_4/TiO_2-B(001) heterostructures can be fabricated in several ways, for example, stacking with different contact sites or with different orientations. However, the criterion of heterostructure construction is to have a small lattice mismatch because a favorable interface structure requires a small lattice mismatch, which can maximize the orbital overlap between separated components. Based on this requirement, several possible heterostructure configurations can be constructed. But, after lattice match screening, geometrical models of g-C_3N_4/TiO_2-B(001) heterostructures with the least lattice mismatch are shown in Fig. S1. g-C_3N_4/TiO_2-B(001) heterostructure, $A_1 \times A_2$ g-C_3N_4 supported by $B_1 \times B_2$ TiO_2-B(001) surface, is fabricated by artificial rotation, where $A_1 = 2a_1$, $A_2 = a_1 + a_2$, and $B_1 = b_1 + b_2$, $B_2 = b_1 - b_2$. Here, a_1, a_2 and b_1, b_2 are lattice vectors of clean g-C_3N_4 and TiO_2-B(001), respectively. To examine the compatibility of the interface between g-C_3N_4 and TiO_2-B(001) surfaces, lattice mismatch is calculated. The lattice mismatch is defined as $\delta = (b_0 - a_0)/a_0$, where b_0 is the lattice constant of TiO_2-B(001) surface (i.e., $b_{0,1} = 3.76$Å and $b_{0,2} = 12.77$Å), and a_0 is the lattice constant of g-C_3N_4 (i.e., $a_0 = 7.17$Å). A positive value indicates that the g-C_3N_4 monolayer is stretched, and a negative value indicates that the g-C_3N_4 monolayer is compressed. Our calculated δ values for lattice constant a_0 and b_0 of the g-C_3N_4/TiO_2-B(001) heterostructure are -0.14% and -1.76%, respectively, indicating that the g-C_3N_4 monolayer is under compressive strain. Note that the lattice vector angle of TiO_2-B(001) is 31.61°, which is slightly larger than that of g-C_3N_4. We adopt a 30° angle between the lattice vectors in order to facilitate the construction of the heterojunction structure. From our calculations, we can see that the lattice mismatch in current calculations is acceptable.

The top- and side-view of g-C_3N_4/TiO_2-B(001) and Li-F co-doped g-C_3N_4/TiO_2-B(001) heterostructures are shown in Fig. S1(c) and (d). To facilitate the presentation of the surface interface structure of the heterojunction, we have re-cut the supercell unit (black dash box), as shown in Fig. S1(c) and (d).

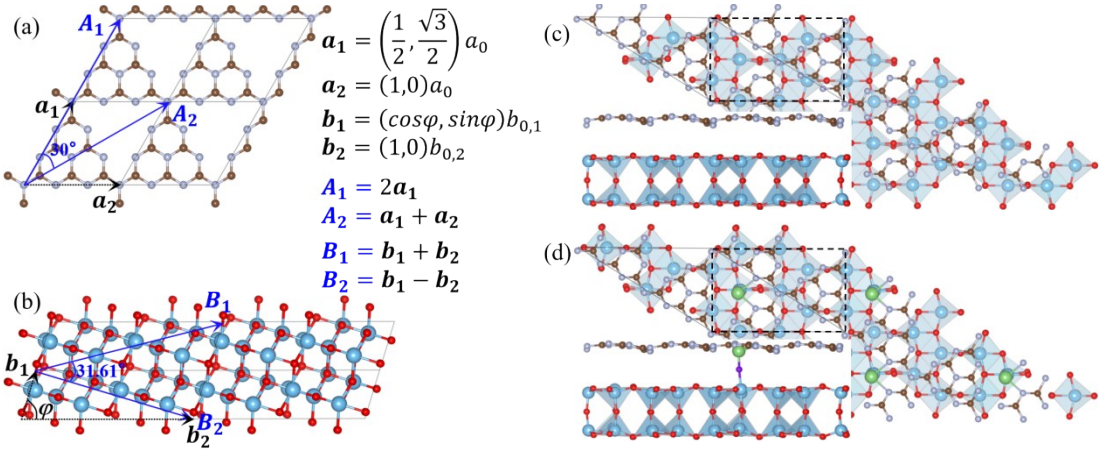

Fig. S1. Schematic diagram of supercell construction for g-C_3N_4/TiO_2-B(001) heterostructure. (a) Geometry and unit cell of g-C_3N_4. (b) Geometry and unit cell of TiO_2-B(001) surface. (c)-(d) Top- and side-view of g-C_3N_4/TiO_2-B(001) and Li-F co-doped heterostructures. Note that the black dash boxes are supercells used in the main body text. Gray, brown, blue, red, green, and purple spheres represent N, C, Ti, O, Li, and F atoms, respectively. The lattice constant of primitive cell g-C_3N_4 is a_0 =7.17Å and the lattice constants of TiO_2-B(001) are $b_{0,1}$ =3.76Å and $b_{0,2}$ =12.77Å.

2. Geometries of water on various TiO_2-B(001) surfaces

Based on the principle of matching the structure of adsorbates with the substrate, the molecular adsorption and dissociative adsorption configurations of water molecules on different TiO_2-B surfaces were constructed. Fig. S2 illustrates the most stable adsorption and dissociation configurations of water on different TiO_2-B(001) surfaces. As one can see from Fig. S2, the Ti^*_{5c}(Ti13) site exhibits the lowest adsorption energy for water on the pristine and Li-F co-doped TiO_2-B(001)/g-C_3N_4 heterostructures. Consequently, the dissociation adsorption energy of water molecules was optimized and calculated using Ti13 site as the reference configuration in the main text.

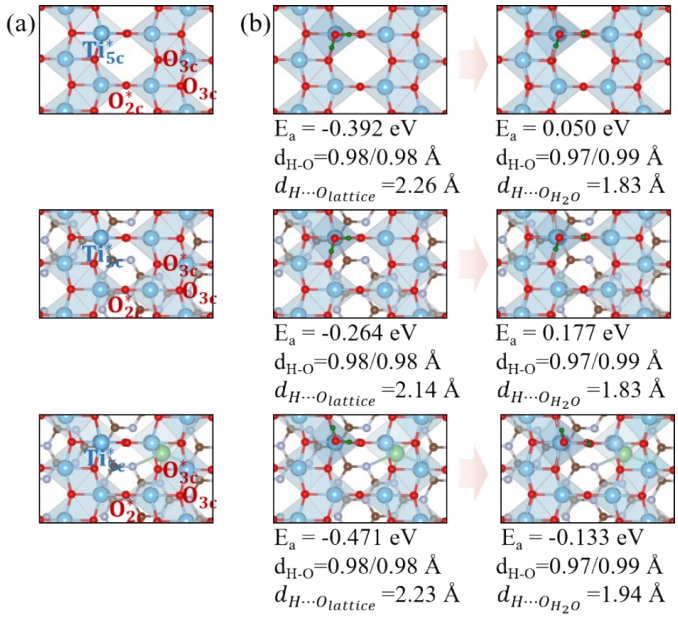

Fig. S2. (a) Surface structural features of TiO_2-B(001), TiO_2-B(001)/g-C_3N_4 and Li-F co-doped TiO_2-B(001)/g-C_3N_4. (b) The most stable configurations for molecule adsorption and dissociated adsorption of water on various TiO_2-B(001) surfaces. Ti^*_{5c} is the primary active site for water adsorption. Adsorption energies and structural parameters are also given below each geometry.

3. Geometries of proton on TiO_2-B(001) surfaces

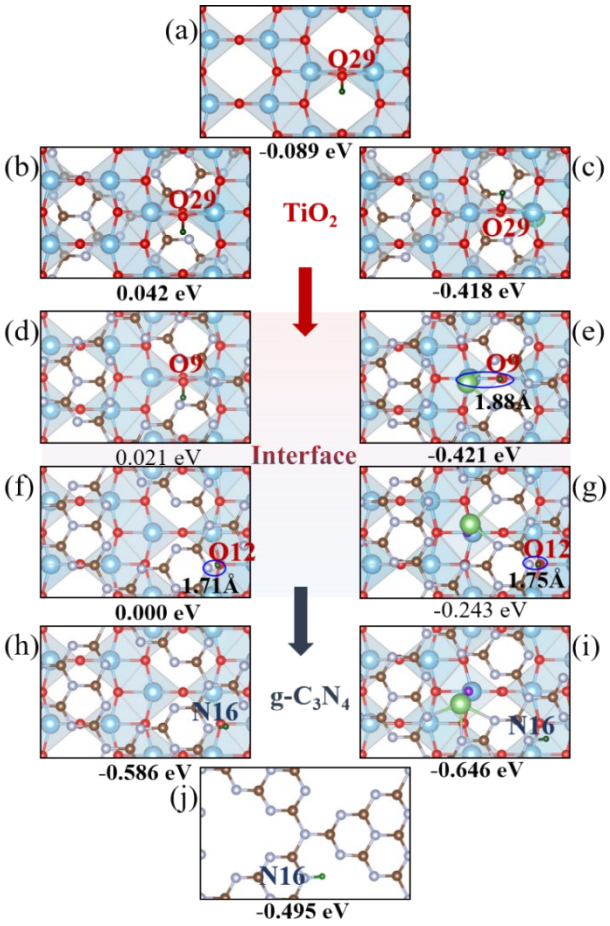

Fig. S3. (a)-(c) The most stable adsorption configurations of proton on O_{2c}^{*} site (labeled as O29) on different TiO_2-B(001) surfaces. (d)-(g) The most stable adsorption configuration candidates of proton on O_{2c}^{*} site (labeled as O9) or O_{3c} site (labeled as O12) at the interfaces. (h)-(j) The most stable adsorption configurations of proton on pyridine nitrogen (labeled as N16) on g-C_3N_4 surface. Adsorption energies are also given below each geometry.

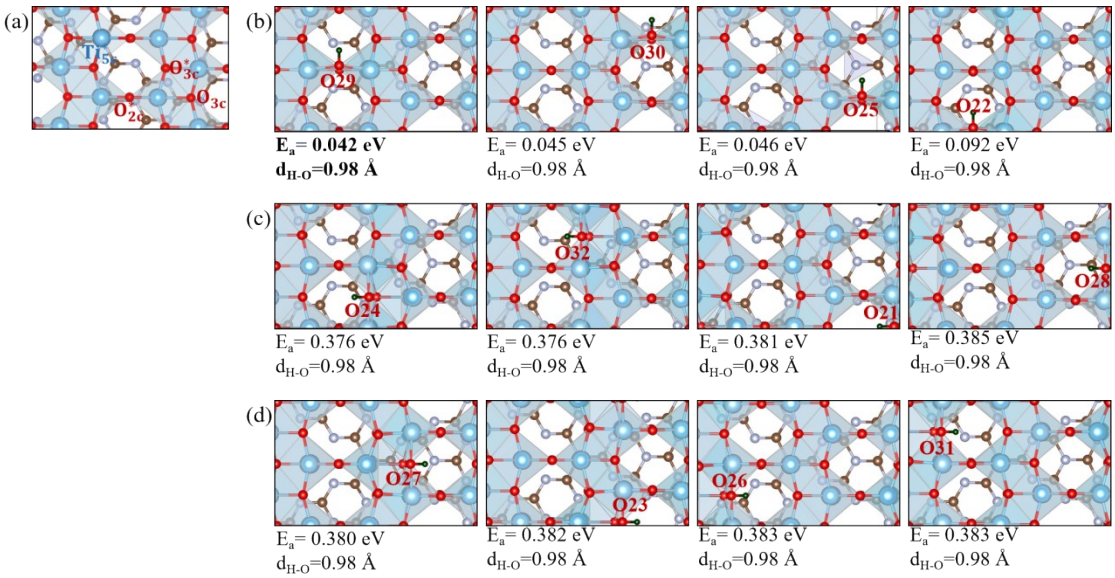

Fig. S4. (a) Some possible adsorption sites of proton on surface of TiO_2-B(001)/g-C_3N_4 heterostructure, i.e., Ti^*_{5c}, O^*_{2c}, O^*_{3c}, and O_{3c}site. (b) Geometries of proton on O^*_{2c} site, i.e., O29, O30, O25, and O22. (c) Geometries of proton on O_{3c} site, i.e., O24, O32, O21, and O28. (d) Geometries of proton on O^*_{3c} site, i.e., O27, O23, O26, and O31. Adsorption energy and bond length are given below each geometry.

4. Geometries of proton on interface of TiO_2-B(001) heterostructure

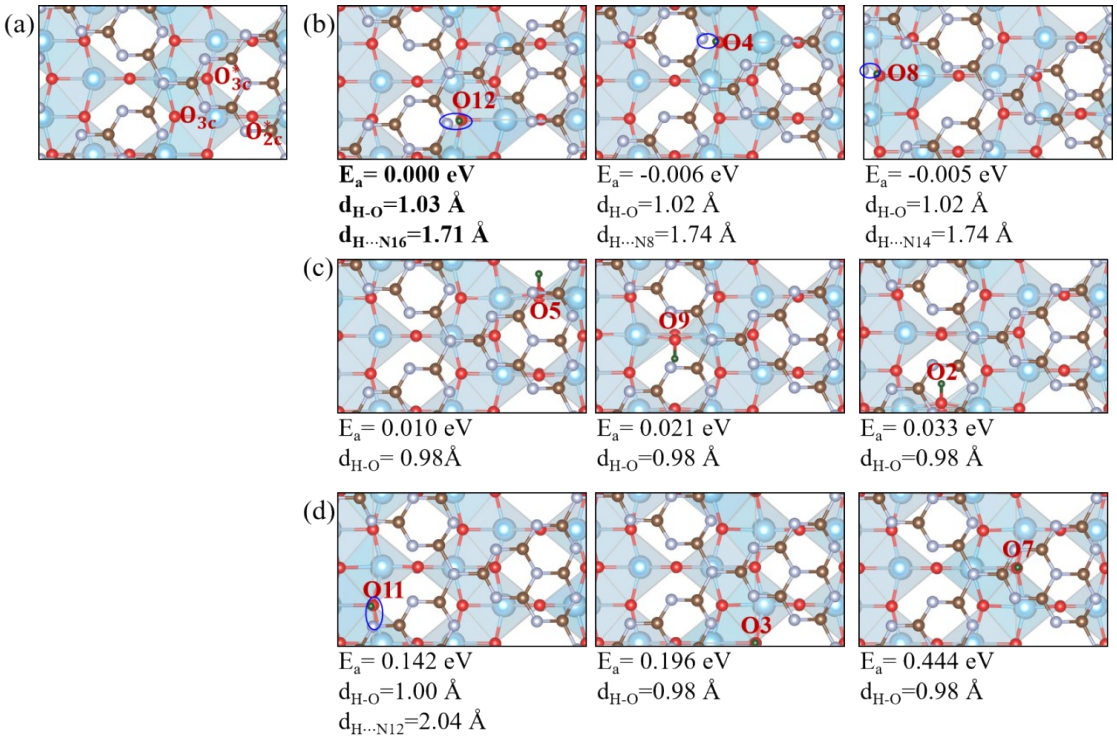

Fig. S5. (a) Some possible adsorption sites of proton at interface of TiO_2-B(001)/g-C_3N_4 heterostructure, i.e., O^*_{2c}, O^*_{3c}, and O_{3c}site. (b) Geometries of proton on O_{3c} site, i.e., O12, O4, and O8. (c) Geometries of proton on O^*_{2c} site, i.e., O5, O9, and O2. (d) Geometries of proton on O^*_{3c} site, i.e., O11, O3, and O7. Adsorption energy and bond length are given below each geometry.

5. Geometries of proton on TiO_2-B surface in Li-F co-doped heterostructure

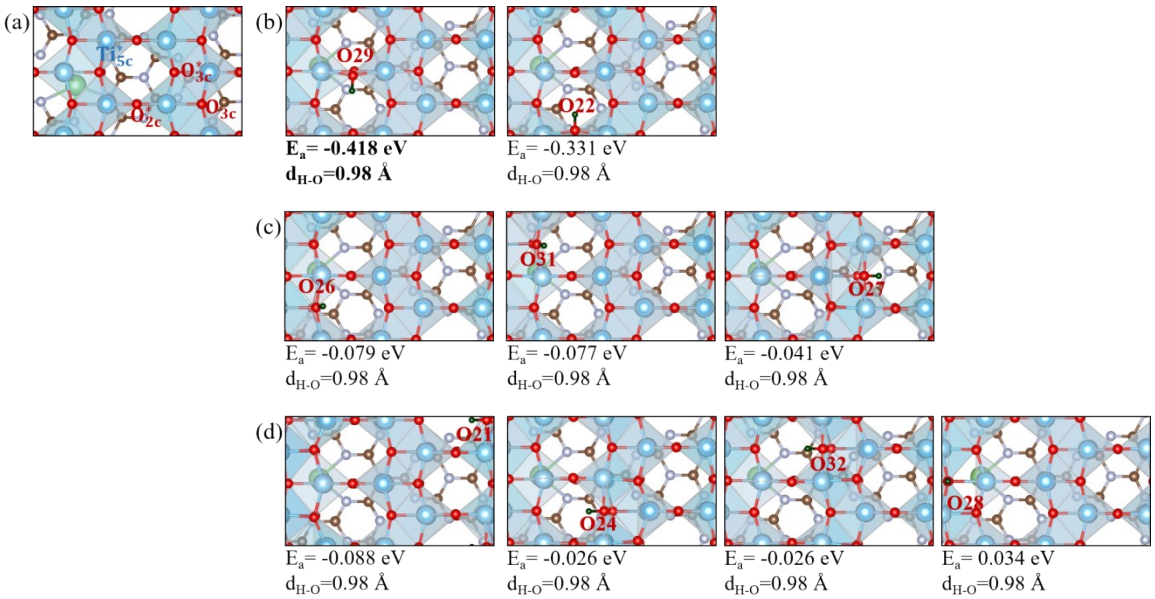

Fig. S6. (a) Some possible adsorption configurations of protons on the surface of Li-F co-doped TiO_2-B(001)/g-C_3N_4 heterostructures, i.e., Ti^*_{5c}, O^*_{2c}, O^*_{3c}, and O_{3c} site. (b) Geometries of proton on O^*_{2c} site, i.e., O29 and O22. (c) Geometries of proton on O^*_{3c} site, i.e., O26, O31, and O27. (d) Geometries of proton on O_{3c} site, i.e., O21, O2, O32, and O28. Adsorption energy and bond length are given below each geometry.

6. Geometries of proton at the interface of Li-F co-doped heterostructure

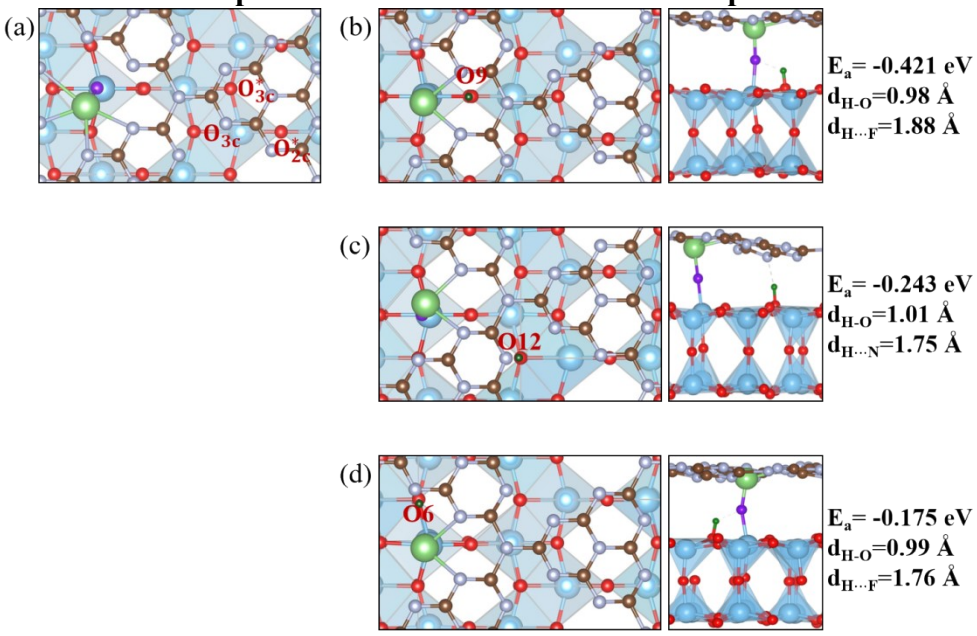

Fig. S7. (a) Some possible adsorption sites of protons at the interface of Li-F co-doped TiO_2-B(001)/g-C_3N_4 heterostructure, i.e., O^*_{2c}, O^*_{3c}, and O_{3c}site. (b) Geometries of proton on O^*_{2c} site, i.e., O9. (c) Geometries of proton on O_{3c} site, i.e., O12. (d) Geometries of proton on O^*_{3c} site, i.e., O6. Adsorption energy and bond length are given below each geometry.

7. Geometries of proton on different g-C_3N_4 surfaces

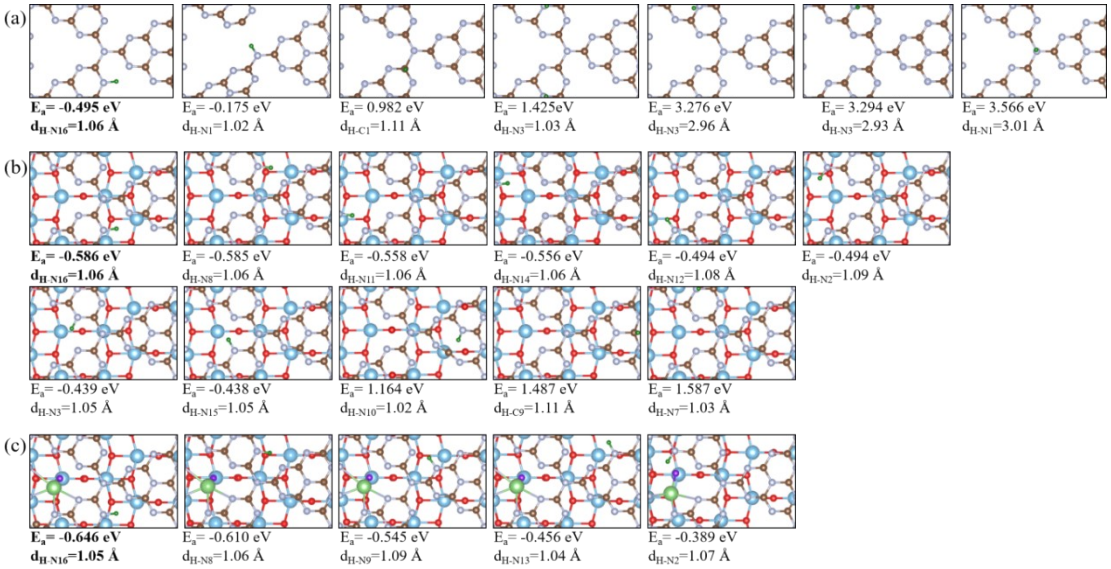

Fig. S8. Some possible adsorption configurations of proton on various g-C_3N_4 surfaces. (a) g-C_3N_4 surfaces. (b) g-C_3N_4/TiO_2-B(001) surface. (c) Li-F co-doped g-C_3N_4/TiO_2-B(001) surface. Pyridine N (labeled as N_2) is the primary adsorption site for proton. The typical pyridine nitrogen is at the N16 site. Adsorption energy and bond length are given below each geometry.

8. Confirmation of rate-determining steps

Table S1. Energy barriers for proton migration across the interface or interface diffusion in pristine TiO_2-B/g-C_3N_4 and Li-F co-doped TiO_2-B/g-C_3N_4 heterostructures (at U = 0 V vs. RHE, pH = 0).

Step		**Pristine (eV)**	**Li-F co-doped (eV)**
Water dissociation		0.442	0.338
Proton migration	TiO_2-B→interface	1.103	0.999
	Interface diffusion	–	0.701
	Interface→g-C_3N_4	0.168	0.226
Volmer		–	–
Heyrovsky		0.58	0.65

9. Comparison of migration barrier for proton

Table S2. Proton migration/transfer barriers in various systems.

System	Proton migration step	Energy barrier (eV)	Reference
g-C_3N_4/TiO_2-B(001)	TiO_2-B surface → interface	1.103	Current work
Li-F codoped g-C_3N_4/TiO_2-B(001)	TiO_2-B surface → interface	0.999	Current work
Pt10/TiO_2 (rutile)	Pt_{10}/TiO_2 interface	0.30	Ref. 1
$BaZrO_3$	interstitial of ZrO_6 octahedron	0.19~0.30	Ref. 2
$BaFeO_3$	interstitial of FeO_6 octahedron	0.22	Ref. 3
$CaMnO_3$	surface→bulk surface→bulk	0.66 1.57	Ref. 4

10. References

1. Sun R, Wang R, Liu, X et al. Hydrogen Production on Pt/TiO2: Synergistic Catalysis between Pt Clusters and Interfacial Adsorbates, J. Phys. Chem. Lett., 2022, 13, 3182−3187.

2. Winterhoff G, Neitzel-Grieshammer S. A review of proton migration and interaction energies in doped barium zirconate. Solid State Ionics, 2023, 397, 116231.

3. Hoedl M F, Chesnokov A, et al. Proton migration barriers in BaFeO3−δ – insights from DFT calculations. J. Mater. Chem. A, 2023, 11, 6336.

4. Grimm B and Bredow T. Theoretical Study on Proton Migration on the CaMnO3 Surface. J. Phys. Chem. C, 2024, 128, 12792−12798.